Dynamical Behavior of Multivariate Time Series for SOI, Precipitation/Temperature in Fukuoka and Its Prediction by Artificial Neural Networks

Jin, Young-Hoon
Institute of Environmental Systems : Graduate Student

Kawamura, Akira

Jinno, Kenji
Institute of Environmental Systems : Graduate Student

Iseri, Yoshihiko
Institute of Environmental Systems : Graduate Student

出版情報：九州大学工学紀要. 64 (1), pp.45-62, 2004-03. 九州大学大学院工学研究院
バージョン：
権利関係：

Memoirs of the Faculty of Engineering, Kyushu University, Vol. 64, No. 1, March 2004

Dynamical Behavior of Multivariate Time Series for SOI, Precipitation/Temperature in Fukuoka and Its Prediction by Artificial Neural Networks

by

Young-Hoon JIN*, Akira KAWAMURA**, Kenji JINNO***
and Yoshihiko ISERI****

(Received December 17, 2003)

Abstract

Large atmospheric circulation has affected local/regional hydro-meteorological variables such as precipitation and temperature. The large-scale circulation represented by Southern Oscillation Index (SOI) in the present study has played a driving force affecting the local variables. The underlying interaction among them is difficult to detect directly due to the existence of noise and strong nonlinearity. In the present study, simultaneous predictability of SOI, precipitation, and temperature at Fukuoka was verified through noise reduction by low pass filtering and training of artificial neural networks (ANNs), presenting remarkable properties that can represent the nonlinearity in a system. Two types of transfer function (i.e., hyperbolic tangent and pure linear functions) were applied to hidden nodes, while only pure linear function was used for output layer. Possible extrapolation beyond the extreme values in training was verified with the testing and validation datasets. The observed and predicted values for the two cases were depicted in three-dimensional phase space to reveal the dynamical behavior of the interaction among the regional driving force and local hydro-meteorological variables, as well as shown in the respective time series plots. The identified parameters from training of ANNs were verified in the testing and validation phase as well.

Keywords: Southern Oscillation Index (SOI), Precipitation, Temperature, Artificial neural networks (ANNs), Prediction, Extrapolation, Transfer function

* Graduate Student, Institute of Environmental Systems
** Associate Professor, Institute of Environmental Systems
*** Professor, Institute of Environmental Systems
**** Graduate Student, Institute of Environmental Systems

1. Introduction

El Niño results from a large scale weakening of the trade wind and warming of sea surface temperature in the eastern and central equatorial Pacific. The phenomenon of El Niño lasts typically 12～18 months and occurs irregularly at 2～7 year intervals. In contrast, La Niña phenomenon refers to the condition of lower sea surface temperature than normal. There is an inter-annual seesaw phenomenon that is called Southern Oscillation (SO) in tropical sea level pressure between the eastern and western hemispheres. The Southern Oscillation Index (SOI), which is defined as the normalized difference in surface pressure between Papeete at Tahiti in central Pacific Ocean and Darwin in northern Australia, is a measure of the strength of the trade winds. The features are collectively known as the El Niño/Southern Oscillation (ENSO) phenomenon.

During the latest several decades there has been considerably interested in the influence of ENSO on regional/local hydro-meteorological variables, such as temperature, precipitation, and streamflow, etc[1),2),3)]. These studies showed that the influence of ENSO on hydro-meteorological variables in the lower to mid-latitudes appears evident. For middle to high latitudes the impact of ENSO on local variables is not clear. However, some studies have also shown effects of La Niña and SO on hydro-meteorological variables for the region[4),5)]. For south-east Asia, several studies have been made. One of them studied relationships between SOI and precipitation in the Philippines/Malaysia and Japan, respectively[6)]. Although no quantitative relationship was calculated, a clear pattern similarity between SOI and precipitation in the Philippines and Malaysia could be found. Kawamura et al. detected quantitative and statistically significant correlation between SOI and precipitation/temperature in Japan, using a simple but efficient method in which SOI data were categorized into five groups according to their magnitudes[7),8)]. The categorization method was used to reveal the ENSO-influence on precipitation in Busan, Korea[9)].

As described above, the ENSO-influence has been considered as it has played a driving force affecting local climate variation. The ENSO has been approved that it causes disasters such as flood and drought with far distance by teleconnection. Vast losses by the disasters are usually beyond human ability and have arisen with massive property damage and a heavy toll of lives. Therefore, it is very important to understand how the regional driving force has influenced the local variables.

The clear necessity of the research on ENSO-influence motivated this study. The better understanding of the influence might prevent disasters from flood and drought caused by the regional driving force. However, so far, there is little research showing the behavior of the interaction between the regional driving force and local variables in time. The underlying interaction among them is difficult to detect directly due to the existence of noise and strong nonlinearity.

Therefore, in the present study, low pass filtering is applied to reduce the noise from the used data. The low pass filter is especially designed to reduce high-frequency components of the time series, which are usually regarded as noise[10)]. Also, artificial neural networks (ANNs) are used to represent the strong nonlinearity among variables and to reveal how the relationship is changing dynamically in three-dimensional phase space.

Recently, ANNs have become extremely popular for prediction and forecasting in various fields, such as finance, power generation, medicine, water resources and environmental science. The use of neural networks offers very useful properties such as nonlinearity, input-output mapping, and adaptivity[11)]. In particular, the vast applications of ANNs to

water resources, along with outlined steps to be followed for their development, are listed in a paper of Maier et al., [12]. Identification of inputs for multivariate artificial neural network models can be referred to the previous study of the authors[13].

The remarkable properties of ANNs are used in the present study to present the nonlinear relationship between SOI as a regional driving force and local hydro-meteorological variables. Input data used for the present study are the noise-reduced SOI, precipitation, and temperature at Fukuoka. Two models of ANNs are structured with the same number of input, hidden, and output nodes, but different transfer functions in hidden layer. One of the two models shows possibility of extrapolation beyond the extremes in training dataset.

The two models of ANNs carry out the one-step ahead prediction to show simultaneous predictability using the three variables. Both observed and predicted values from training, testing and validation are shown in a three-dimensional phase space to depict how the variables have been evolved dynamically. The ANNs model includes the influence of the regional driving force on local hydro-meteorological variables and their interaction among all of the three variables as well.

2. Data Used

SOI, precipitation, and temperature at Fukuoka were used to verify the simultaneous predictability of multivariate time series using artificial neural networks (ANNs). Fukuoka station was selected since it had long well recorded precipitation and temperature data. The periods of each data were from January 1890 to December 2000. Annual mean precipitation/ temperature values are 1627 mm/ 15.6 °C during the periods, respectively. Time series plots

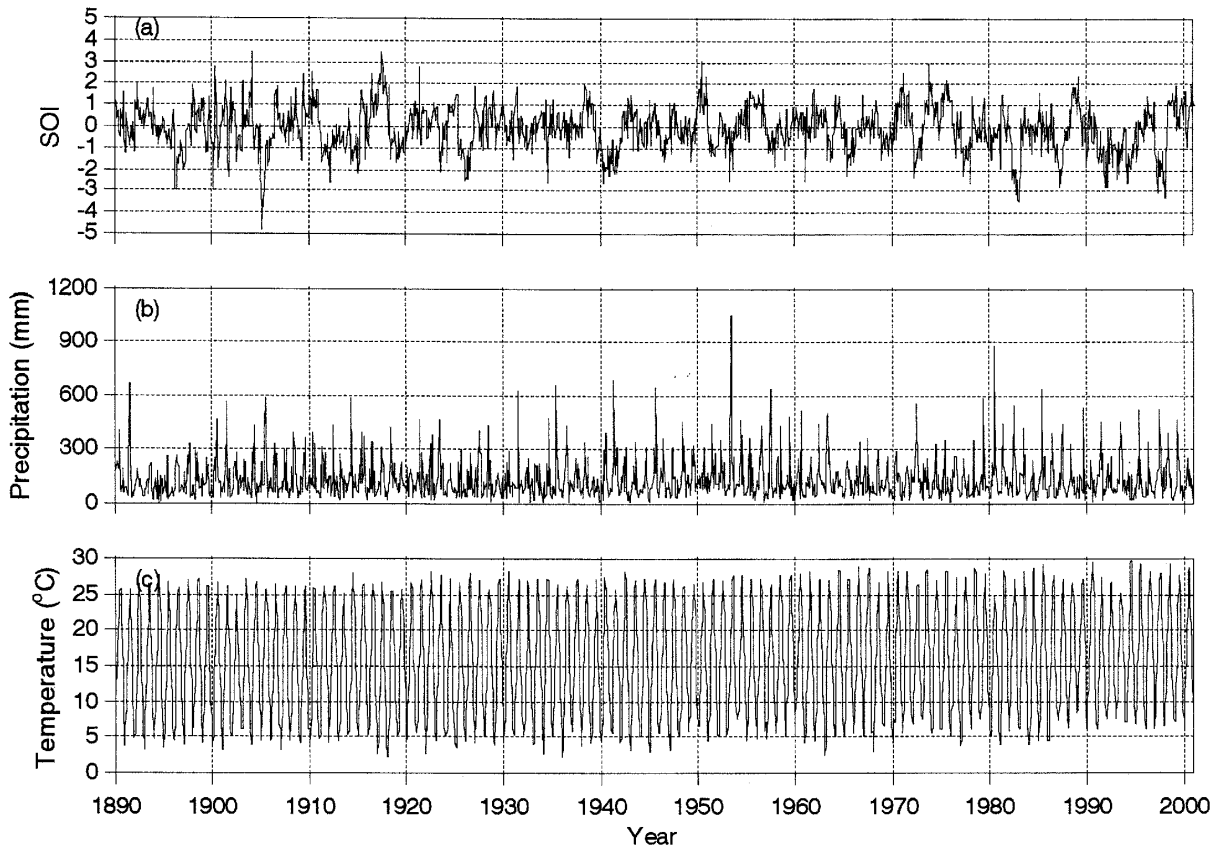

Fig. 1 Time series plots of raw data for (a) SOI, (b) precipitation, and (c) temperature at Fukuoka.

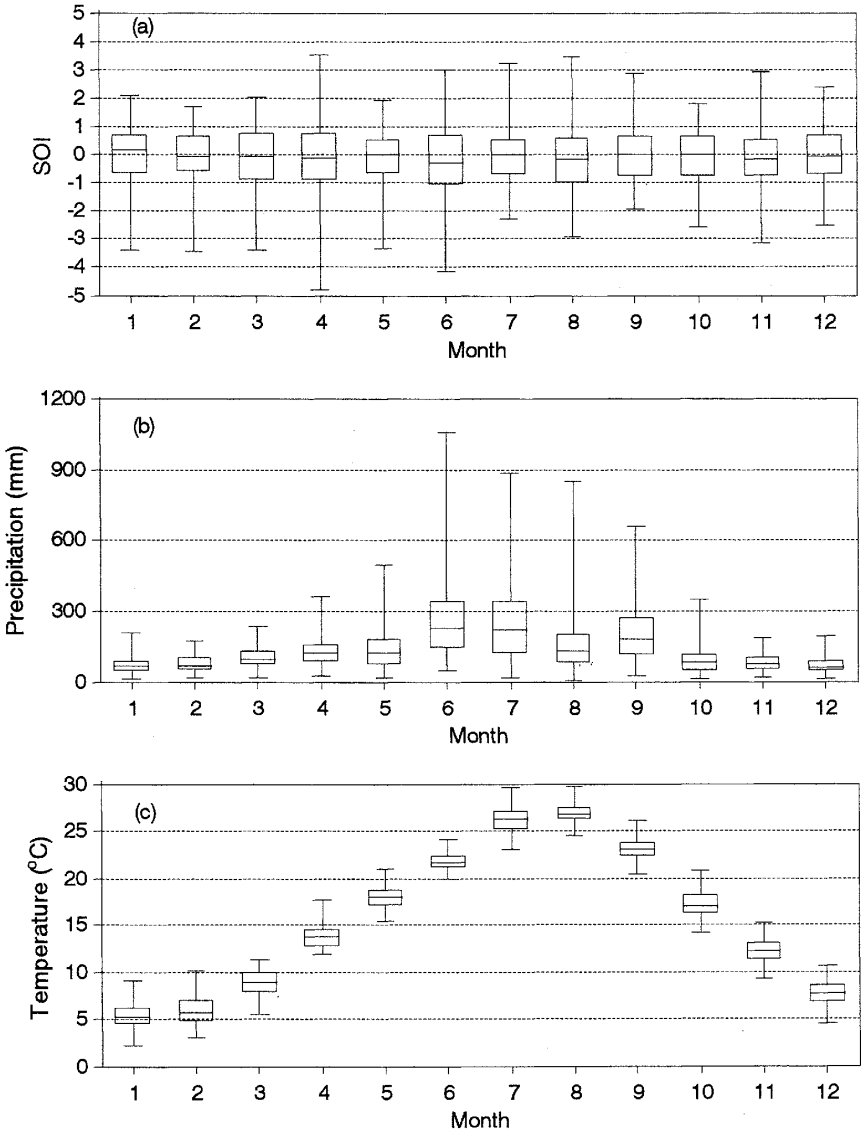

Fig. 2 Box-whisker plots of (a) SOI, (b) precipitation, and (c) temperature at Fukuoka with median, quartiles, maximum, and minimum on a monthly basis.

of the three variables are shown in **Fig. 1**, whereas their box-whisker plots are represented in **Fig. 2** with median, quartiles, maximum, and minimum on a monthly basis. **Figure 2 (a)** represents that SOI data are distributed normally in all months.

However, as is clearly seen in **Fig. 1 (b)**, the time series of precipitation includes a clear periodicity and, in **Fig. 2 (b)**, the distributions of precipitation from January to December reveal high skewness, especially during summer season. Meanwhile, the temperature depicts slight upward trend in the second half of the period in **Fig. 1 (c)** and approximately normal distribution on a monthly basis with the clear periodicity, which is showing an annual cycle as a whole in **Fig. 1 (c)** and **Fig. 2 (c)**. The deterministic components such as periodicity, seasonality, and trend should be removed and, sequentially, the data should be normally standardized to ensure that all variables receive equal attention during the training process in ANNs.

In the present study, the precipitation and temperature were normally standardized using appropriate methods, respectively, while SOI was used as itself because it was already normally standardized (**Fig. 2 (a)**). The precipitation data were normalized by cubic root

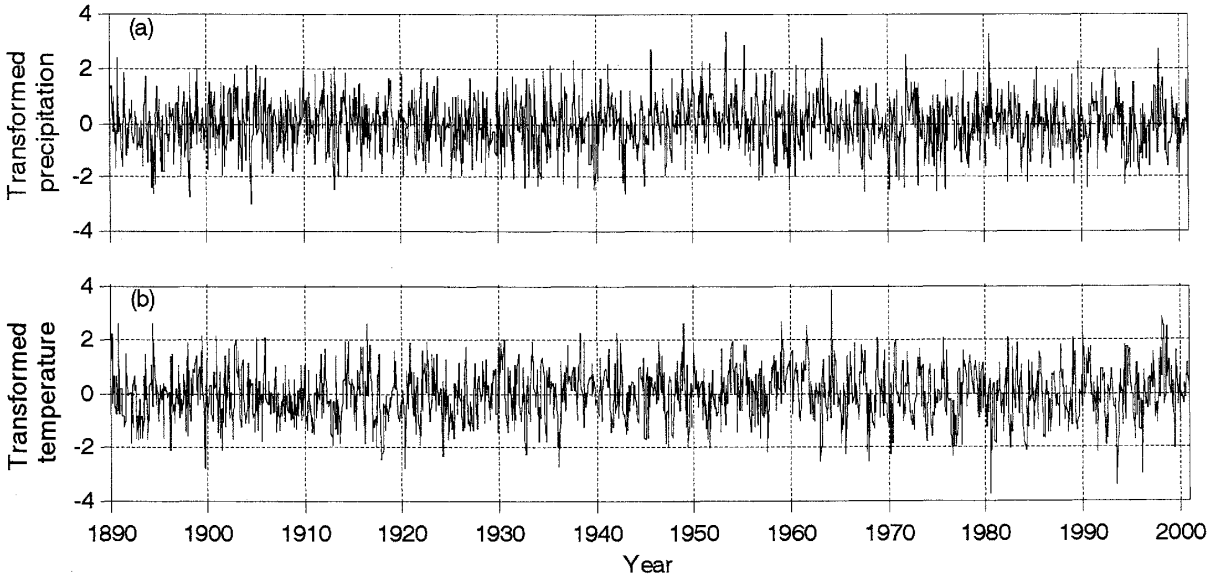

Fig. 3 Transformed (a) precipitation and (b) temperature at Fukuoka.

transformation because its distribution was strongly skewed. The normalized data were, then, standardized into a mean of zero and standard deviation of one, on a monthly basis from January to December (**Fig. 3 (a)**). The temperature data were only standardized into a mean of zero and standard deviation of one, after removing trend after January 1937 from which temperature started to rise, because those were nearly distributed normally (**Fig. 3 (b)**).

In general, observed time series data contain noise. Even though data transformation was used as described above, the noise exists in the time series. Therefore, the time series need to be cleaned by a noise reduction scheme. In the present study, a low pass filter as a linear noise reduction scheme was applied to SOI, precipitation, and temperature time series. A low pass filter is commonly used for noise reduction of any type of time series.

The low pass filter is especially designed to reduce high-frequency components of the time series, which are usually regarded as noise. This scheme used for the present study is expressed as following:

$$y(t)=(1-\alpha)x(t)+\alpha y(t-1) \tag{1}$$

where t is the time step; x is the raw data (in this study, transformed data); y is the smoothed (noise-reduced) data, and α is the smoothing coefficient ($0\leq\alpha\leq1$). Here, α is selected as 0.995, which can make the smoothed values similar to the magnitudes of thirty-year moving average. To obtain data more after noise reduction, the low pass filter is preferred to the thirty-year moving average. The noise reduced time series of SOI, precipitation, and temperature are plotted in **Fig. 4**, respectively, and a three dimensional phase space with the three variables is shown in **Fig. 5**. These datasets are used for inputs in modeling ANNs in the next chapter.

3. Predictability of Artificial Neural Networks (ANNs)

3.1 General theory of ANNs

Generally, the artificial neural network remarkably represents the nonlinear relationship

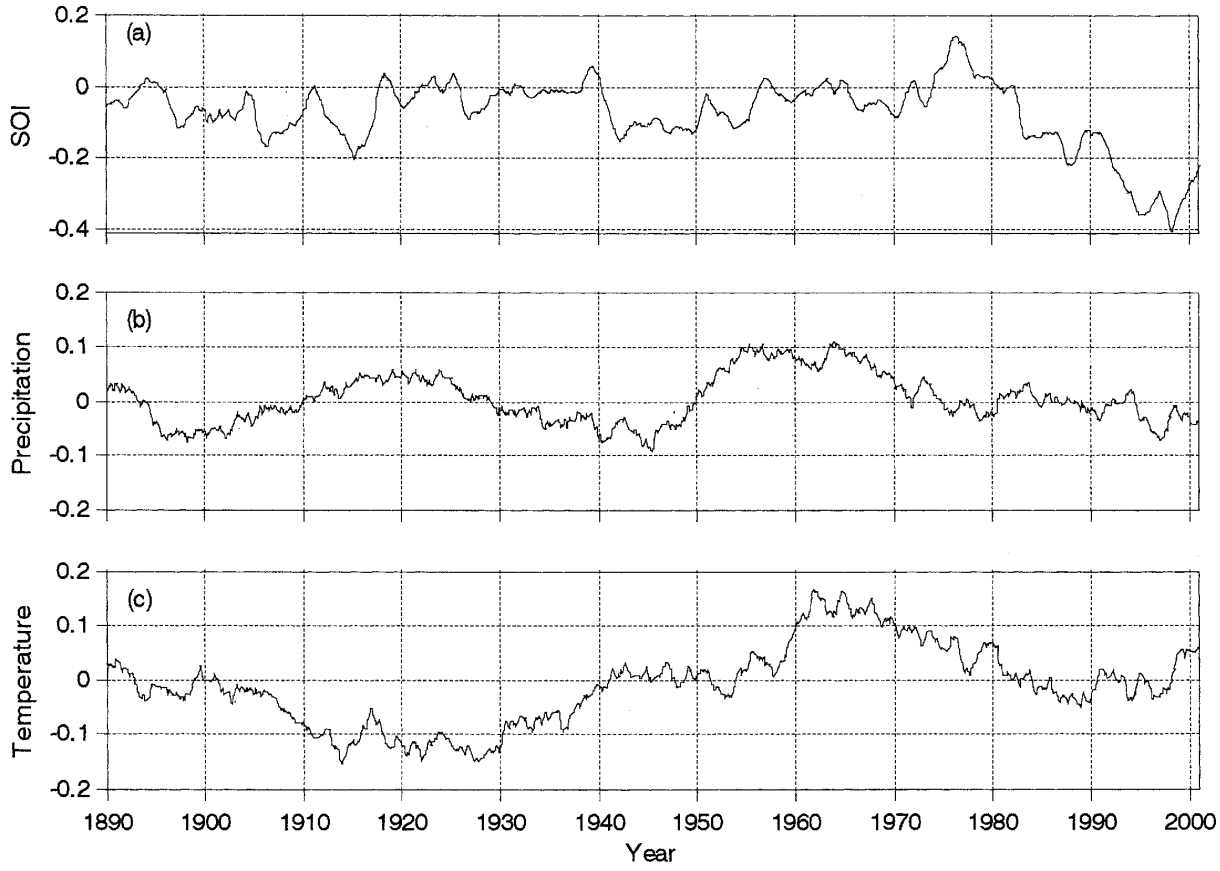

Fig. 4 Noise reduced time series of (a) SOI, (b) precipitation, and (c) temperature, by low pass filter.

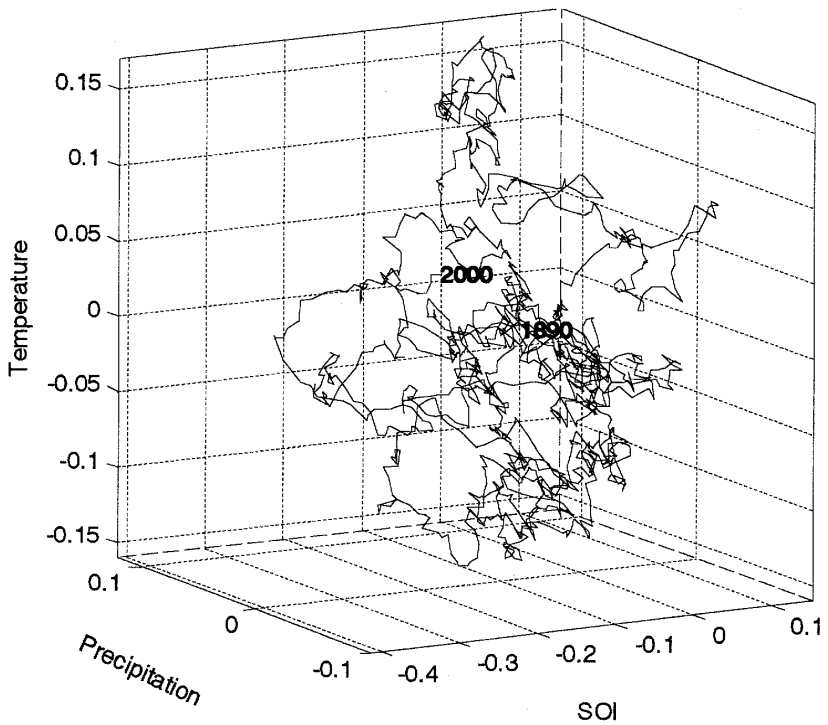

Fig. 5 Three dimensional phase space with noise reduced data of SOI, precipitation, and temperature at Fukuoka.

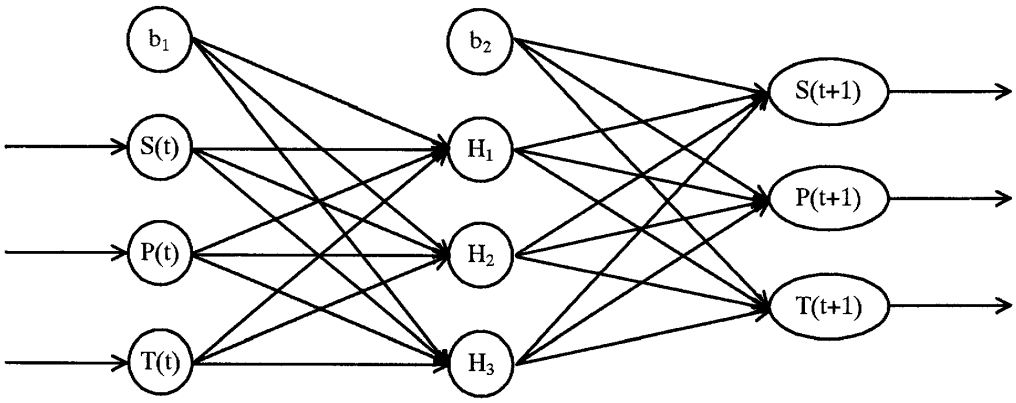

Fig. 6 Architectural graph of the structure used in the present study.

and is well suited to the prediction of the variables based on the nonlinear interaction. For the present study, three input variables with SOI, precipitation and temperature at the present time are used to predict the three values of the next time simultaneously. That is, the prediction is carried out one step ahead. A hidden layer, which can mainly express the nonlinear relationship among the variables, has three nodes. Therefore, the model of the artificial neural network used in the present study has the structure composed of three input, hidden, and output nodes, respectively (**Fig. 6**)

This neural network model performs the usual error back-propagation algorithm for training as a batch mode. In other words, weight updating is performed after all of the training data are presented for computing the output values and this presentation of all the training examples constitutes an epoch. An error from the epoch is calculated as an averaged error from differences between all target and output values. This training method is well known to be very efficient in terms of training speed as well as the training performance.

Briefly describing the error back-propagation algorithm, there are two main procedures to train a neural network: forward and backward passes[11]. In the forward pass, the weights remain unaltered throughout the network, and the function signals of the network are computed on a neuron-by-neuron basis. The induced local field of neuron j, $v_j(n)$ in hidden layer is defined by

$$v_j(n)=\sum_{i=0}^{m} w_{ji}(n)x_i(n) \tag{2}$$

where m is the total number of inputs (excluding the bias, which is represented by $i=0$) applied to neuron j, $w_{ji}(n)$ is the weight connecting neuron i in the input layer to neuron j in hidden layer, and $x_i(n)$ is the input signal of neuron j. The function signal appearing at the output of neuron j in the hidden layer is computed as

$$y_j(n)=\varphi(v_j(n)) \tag{3}$$

The induced local field of neuron k, $v_k(n)$ in hidden output is computed by

$$v_k(n)=\sum_{j=0}^{m} w_{kj}(n)y_j(n) \tag{4}$$

where m, here, is the total number of hidden nodes (excluding the bias) applied to neuron k, $w_{kj}(n)$ is the weight connecting neuron j in the hidden layer to neuron k in output layer, and $y_i(n)$ is the input signal of neuron k or equivalently, the function signal appearing at the output of neuron j. The function signal appearing at the output of neuron k in the hidden

layer is computed as

$$y_k(n)=\varphi(v_k(n)) \tag{5}$$

where $y_k(n)$ is the kth element of the output vector. This output is compared with the desired response, $d_k(n)$, obtaining the error signal $e_k(n)$ for the kth output neuron. Thus, the forward phase of computation begins at the hidden layer by presenting it with the input vector and terminates at the output layer by computing the error signal for each neuron of this layer.

On the other hand, the backward pass starts at the output layer by passing the error signal backward through the network, layer by layer, and recursively computing the δ (i.e., the local gradient) for each neuron. This recursive process permits the weights of the network to undergo changes in accordance with the delta rule defined by

$$\begin{pmatrix} Weight \\ correction \\ \Delta w_{kj}(n) \end{pmatrix}=\begin{pmatrix} learning\text{-}rate \\ parameter \\ \eta \end{pmatrix}\cdot\begin{pmatrix} local \\ gradient \\ \delta_k(n) \end{pmatrix}\cdot\begin{pmatrix} input\ signal \\ of\ neuron\ j \\ y_j(n) \end{pmatrix} \tag{6}$$

For a neuron located in the output layer, the δ is simply equal to the error signal of that neuron multiplied by the first derivative of its nonlinearity. Eq. (6) computes the changes to the weights of all the connections feeding into the output layer. After calculating the δs for the neurons of the output layer, the δs for all neurons in the hidden layer are computed as

$$\delta_j(n)=\varphi'_j(v_j(n))\sum_k \delta_k(n)w_{kj}(n) \tag{7}$$

Therefore, the changes to the weights of all connections are fed into the hidden layer.

3.2 Application of ANNs

As mentioned earlier, the observed data usually contain noise. Therefore, the multivariate time series need to be cleaned by a noise reduction scheme. In the present study, a low pass filter was applied to the time series of SOI, precipitation, and temperature with the smoothing coefficient of 0.995 that can make the smoothed values similar to the magnitudes of thirty-year moving average. The noise-reduced data were used for the input data after scaling the data into the range of [-0.8, 0.8]. Also, the whole data were divided into three subsets for training, testing and validation.

The scaling should be performed in order to ensure that all variables receive equal attention during the training process. In the present study, the scaling was carried out with the training and testing data. In other words, a set of minimum and maximum corresponding the two datasets were used to scale the smoothed data linearly into [-0.8, 0.8], at the same time. Then, the maximum and minimum values were reused to scale the data for validation. That is, the data beyond the extreme values for training and testing procedures can exist in the testing and validation datasets. The distinguishable difference between testing and validation is that the information of testing was used for training phase but no prior knowledge for validation was considered. The period from 1890 to 1940 data was used for training and 1941 to 1970 for testing, while the data of the three variables from 1970 to 2000 were used for validation.

In the present study, the transfer function in hidden the layer took hyperbolic tangent and pure linear functions, whereas the output layer took only a pure linear function. An adaptive learning rate was also used to improve the performance of the training. This adaptive learning rate attempts to keep the learning step size as large as possible while keeping

learning stable and the learning rate in every epoch is made responsive to the complexity of the local error surface. The learning rate was set as 0.7 initially, whereas 0.1 was set for the momentum constant. Training was carried out during a total epoch number of 1000.

4. Results

4.1 Training with hyperbolic tangent function in hidden layer

Figure 7 shows the performance of the network composed for the present study with three input, hidden, and output nodes, respectively. The model used the hyperbolic tangent function in hidden layer. As mentioned earlier, the periods of the respective data for training is from 1890 to 1940. Also, the three input data use the noise-reduced data by low pass filter with α of 0.995. In the present study, the updated weights in training of the artificial neural network are applied for testing and validation in every epoch, as seen in **Fig. 7**.

It reveals that the network was well trained enough with no more decreasing of errors in both training and testing after the specified epoch number. The error in validation also converged into the similar magnitude with the error in testing. Average root mean squared error (RMSE) was around 0.035 for training. Respective results for SOI, precipitation and temperature from training are shown in **Fig. 8** with target (observed values) and predicted values (outputs from network), and their respective RMSEs are shown in for each phase, respectively. As can be clearly seen in the figure, the outputs of the respective variables well predicted the corresponding target values in the training phase.

However, for the results of testing, the respective plots of observed and predicted values for SOI, precipitation, and temperature are shown in **Fig. 9**. RMSE for testing revealed about 0.14, as seen in **Table 1**, when the weights from the trained network were applied to the noise-reduced data of the three variables from 1941 to 1970 in every epoch. As mentioned earlier, a set of minimum and maximum values from training and testing was used for scaling of the corresponding data. The maximum values during the periods were in the data for testing of precipitation and temperature, while it was in training phase for SOI. Therefore, the scaled data for training had no the scaled maximum values for precipitation and temperature.

Sequentially the neural network model was trained using the data with the narrower

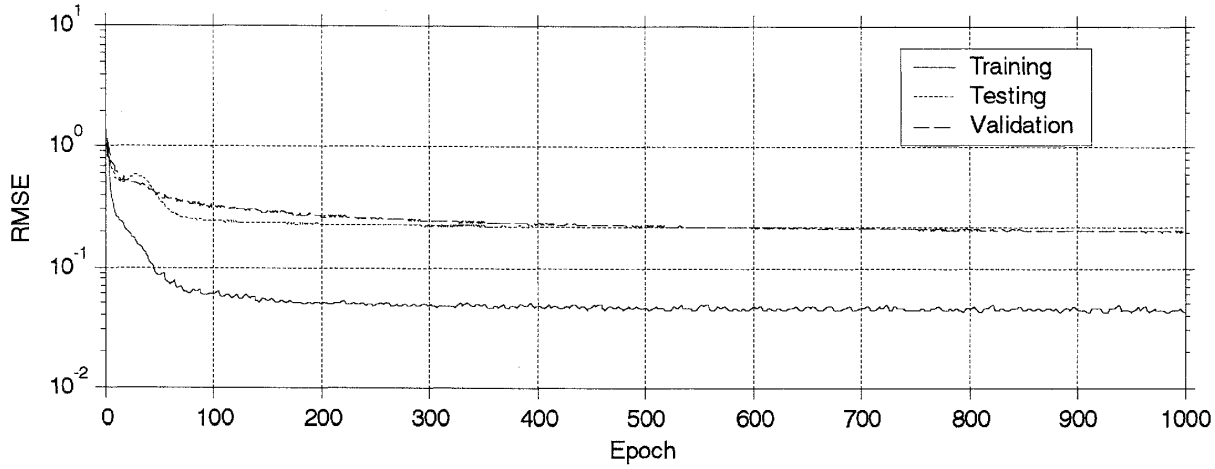

Fig. 7 Performance of artificial neural network with hyperbolic tangent for transfer function in hidden layer composed of three inputs, hidden nodes, and outputs, respectively, with maximum epoch number of 1000.

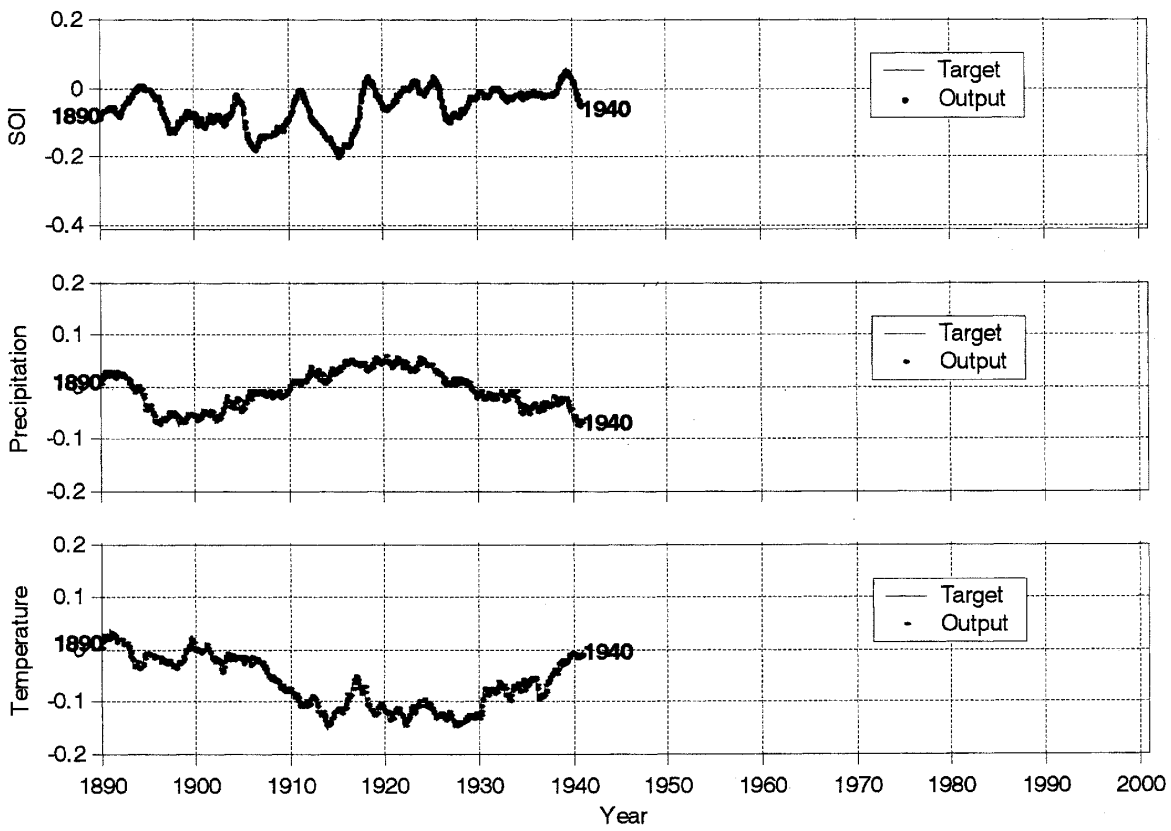

Fig. 8 Observed and predicted values from the artificial neural network with hyperbolic tangent for transfer function in hidden layer in training.

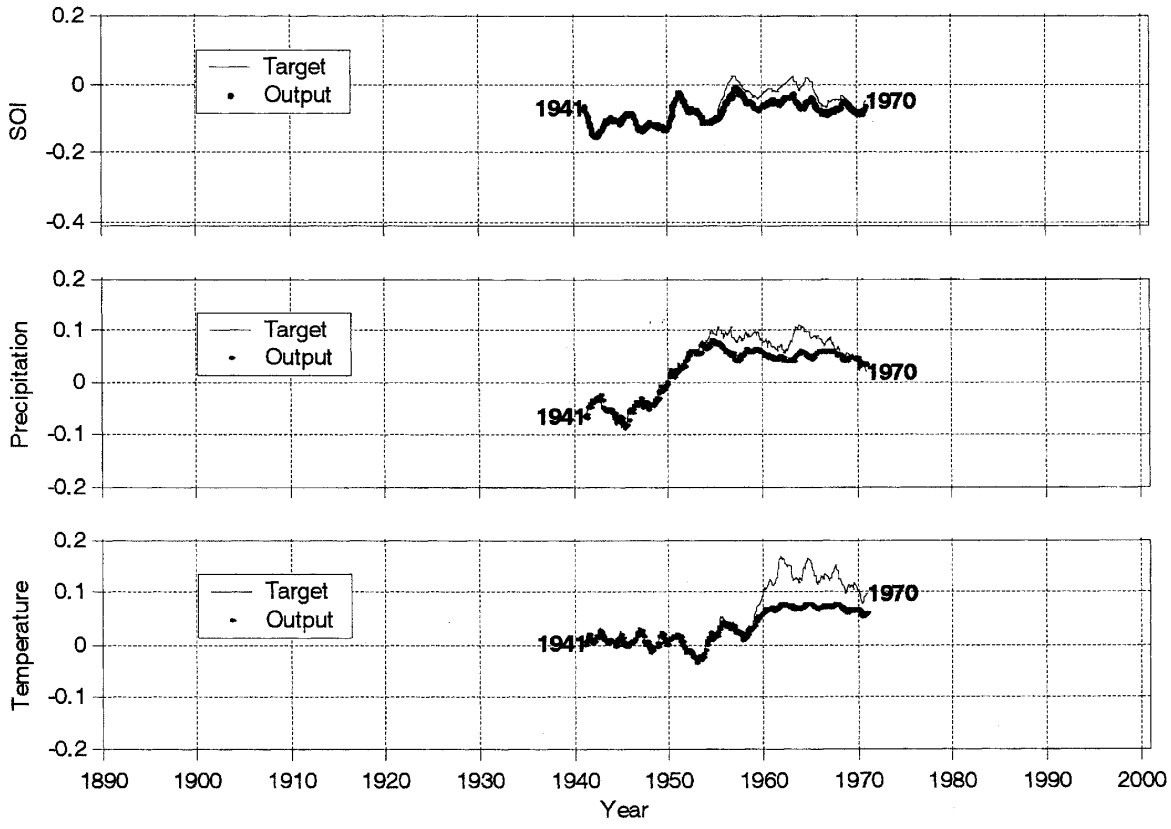

Fig. 9 Observed and predicted values from the artificial neural network with hyperbolic tangent for transfer function in hidden layer in testing.

Table 1 Root mean squared errors (RMSEs) in the respective phases from the model with hyperbolic tangent function for hidden layer.

Phase / RMSE	Training	Testing	Validation
Average RMSE	0.0348	0.1361	0.1734
RMSE for SOI	0.0349	0.1044	0.2580
RMSE for precipitation	0.0423	0.1549	0.1231
RMSE for temperature	0.0249	0.1437	0.0920

range than [-0.8, 0.8] and has lower predictability for the data beyond the range used for training. As clearly seen in **Fig. 9**, there are considerable under-estimating in the second half of the testing data for the respective variables. The average RMSE of three variables is about 0.14 in testing, while the respective RMSEs are shown in **Table 1**. It is considered that the under-estimating for SOI was influenced by low prediction for precipitation and temperature, because the weights in the network was identified from the average RMSE of each error for the three variables simultaneously.

The limited applicability of the parameters identified by the narrow range in training can be clearly seen in **Fig. 10**, which shows the observed and predicted values for validation for the respective variables. Average RMSE of three variables is about 0.17 and the respective RMSEs are about 0.26 for SOI, 0.12 for precipitation, and 0.09 for temperature, as seen in

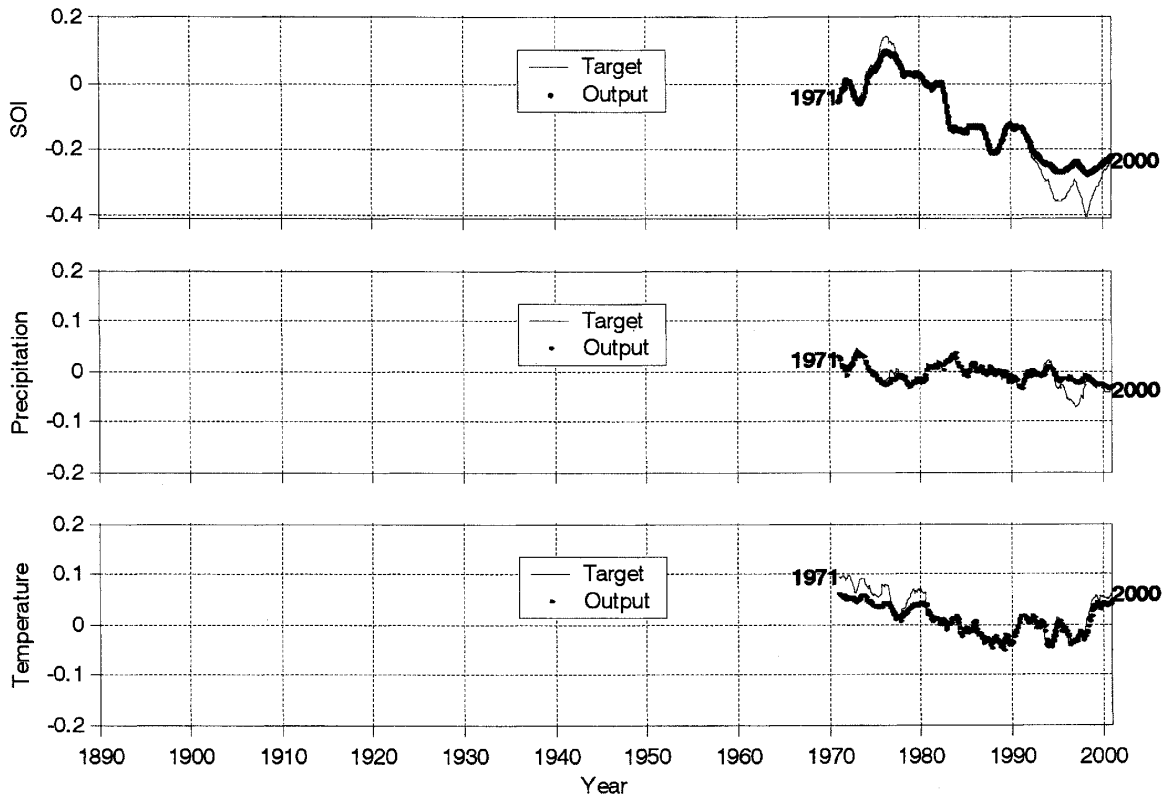

Fig. 10 Observed and predicted values from the artificial neural network with hyperbolic tangent for transfer function in hidden layer in validation.

Table 1. Especially, there is significant under- and over estimation in the validation for SOI, due to the existence of highly extreme values beyond the range in training and testing. The smoothed extreme values for SOI in the whole period used for the present study occurred in 1976 and 1998, respectively. The scaled range of [-2.03, 1.32] for SOI in validation by the minimum and maximum values during training and testing periods considerably exceeds that of [-0.8, 0.8] in training.

Therefore, the problem for extrapolation of the data beyond the range used for training is not trivial but instead critical for the simultaneous prediction of the three variables by ANNs in the present study. In the next section, the alternative using pure linear function in hidden layer for the training of neural network is proposed and the results are described in detail.

4.2 Training with pure linear function in hidden layer

Pure linear function in hidden layer as an alternative to overcome the limitation described above was applied to extrapolate the extreme values beyond the data used in training. The RMSEs with pure linear function in hidden layer are listed in **Table 2** and the variations through epochs were depicted in **Fig. 11** for the respective phases of training, testing, and validation, respectively. As seen in the figure, the RMSEs of the each phase after

Table 2 Root mean squared errors (RMSEs) in the respective phases from the model with pure linear function for hidden layer.

Phase / RMSE	Training	Testing	Validation
Average RMSE	0.0334	0.0366	0.0355
RMSE for SOI	0.0344	0.0331	0.0368
RMSE for precipitation	0.0396	0.0442	0.0419
RMSE for temperature	0.0245	0.0313	0.0259

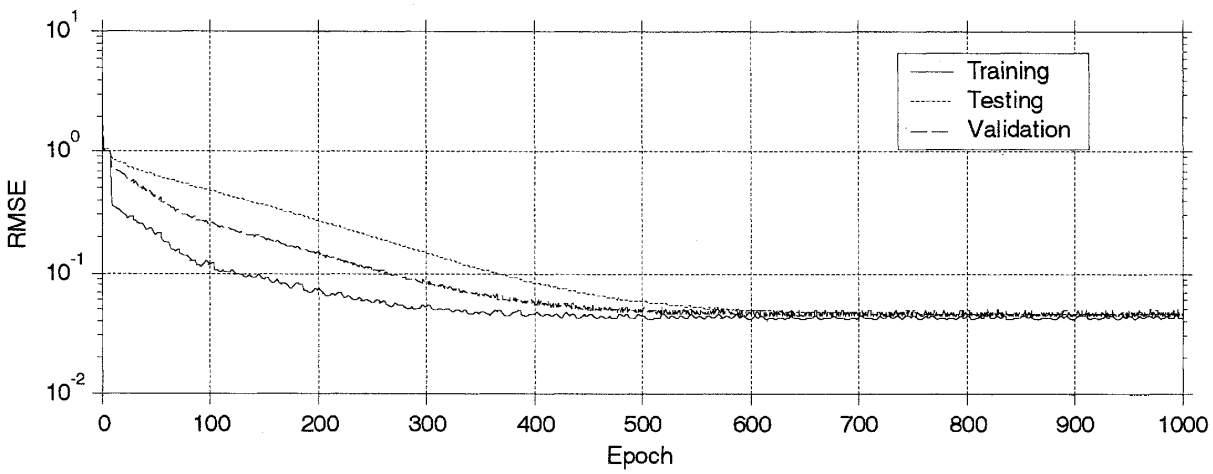

Fig. 11 Performance of artificial neural network with pure linear for transfer function in hidden layer composed of three inputs, hidden nodes, and outputs, respectively, with maximum epoch number of 1000.

the maximum epoch number converged into the similar values listed in **Table 2.**

Compared to the results from the neural network with hyperbolic tangent function in hidden layer, the results with pure linear function in the same layer show significant improvement in the all phases of training, testing, and validation, in general. The observed and predicted values were plotted in **Fig. 12** and three-dimensional phase space was used to depict the dynamical behavior of the interaction among the three variables in **Fig. 13.** It is clear

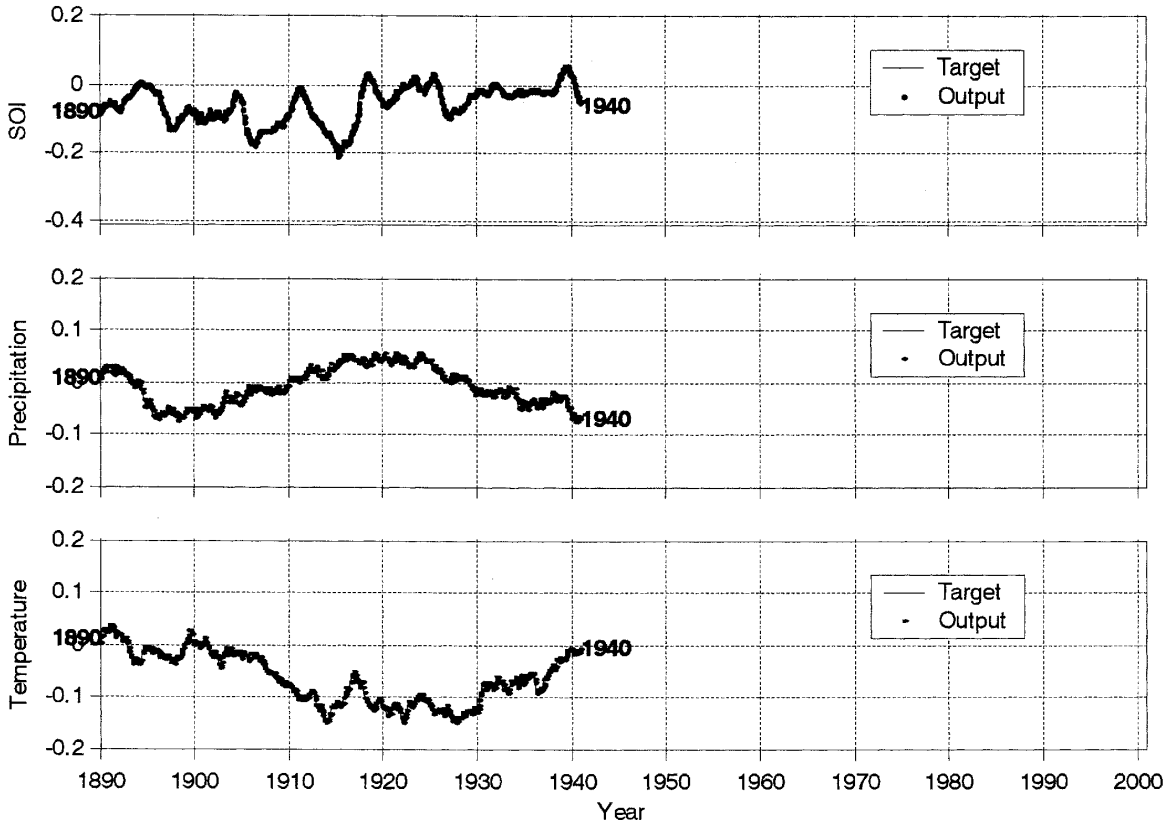

Fig. 12 Observed and predicted values from the artificial neural network with pure linear for transfer function in hidden layer in training.

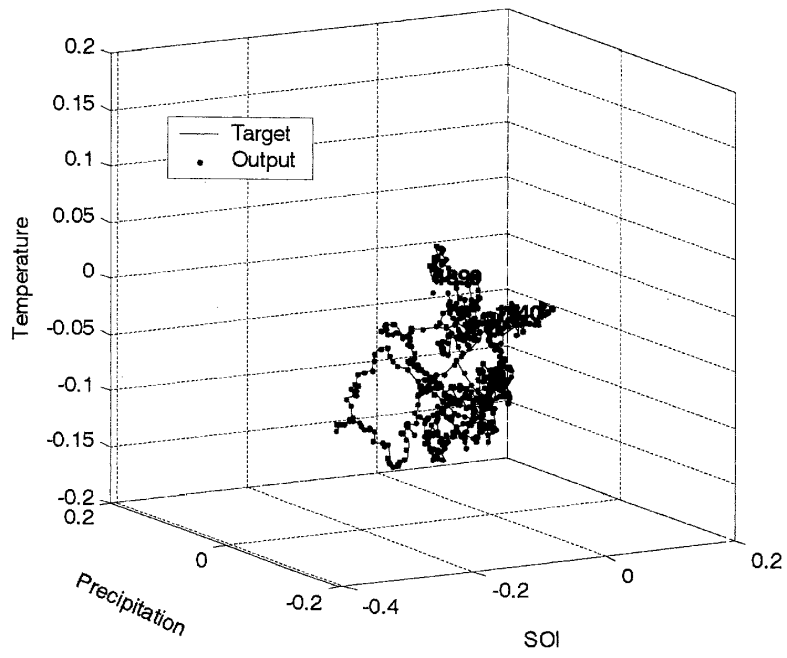

Fig. 13 Three-dimensional phase space representing observed and predicted values in training of the artificial neural network with pure linear for transfer function in hidden layer.

that the neural network performed very well for the one step ahead prediction in training. As clearly seen in **Fig. 13**, even though the interaction among variables is randomly evolving in time, the identified model is well representing the dynamical behavior of the interaction as prediction.

In **Fig. 14**, the observed and predicted data in testing were plotted and reveal the identified model is very well performing for testing as well. Especially, the identified model extrapolated the extreme values beyond the data used for training in testing phase. Also, **Fig. 15** shows the dynamical behavior of interaction among variables in testing and present that the model has the considerable ability of extrapolation for data beyond the range of training. However, it should be note that the information for testing was involved in training phase, i.e., the maximum and minimum values from the dataset for testing could possibly used for training. Therefore, the identified model should be retested with the independent dataset of obtaining the generalized evidence for the model.

Sequentially, validation was carried out with the independent dataset from training procedure and its results were plotted in **Fig. 16** using the observed and predicted data for this phase. Remarkably, the ability for extrapolation of the identified model was represented in this phase, especially for SOI. As mentioned earlier, the range for validation data [-2.03, 1.32] greatly exceeds that for training and testing, [-0.8, 0.8]. Nevertheless, the results from validation phase showed the significant and remarkable ability for extrapolation of the most extreme data beyond the range for training. Also, **Fig. 17** clearly show the model can work well for the one step ahead prediction of the interaction among variables as well as reveal that it can represent the dynamical behavior of the interaction by the prediction.

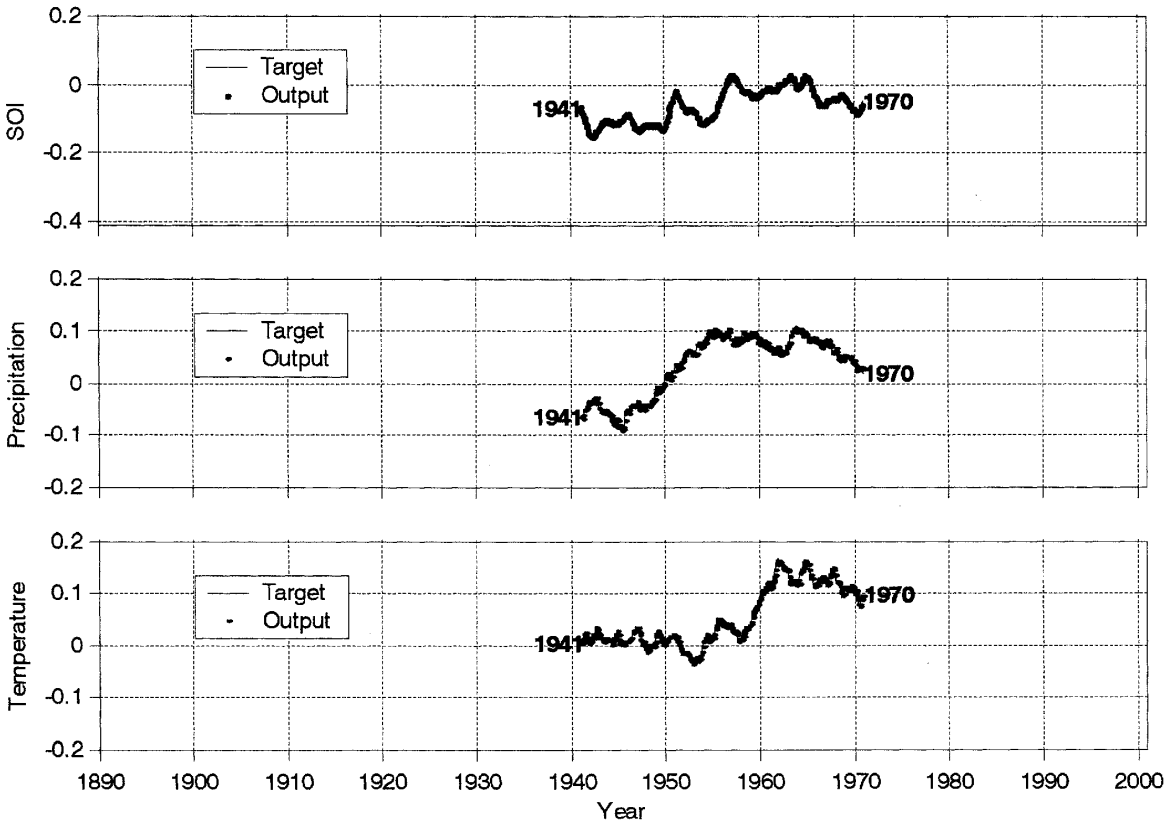

Fig. 14 Observed and predicted values from the artificial neural network with pure linear for transfer function in hidden layer in testing.

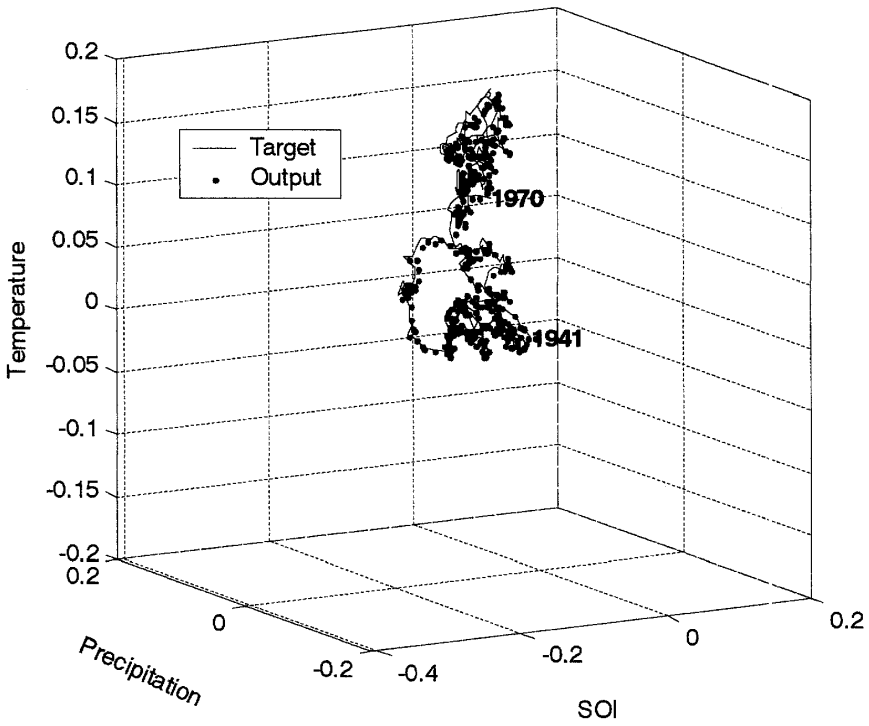

Fig. 15 Three-dimensional phase space representing observed and predicted values in testing of the artificial neural network with pure linear for transfer function in hidden layer.

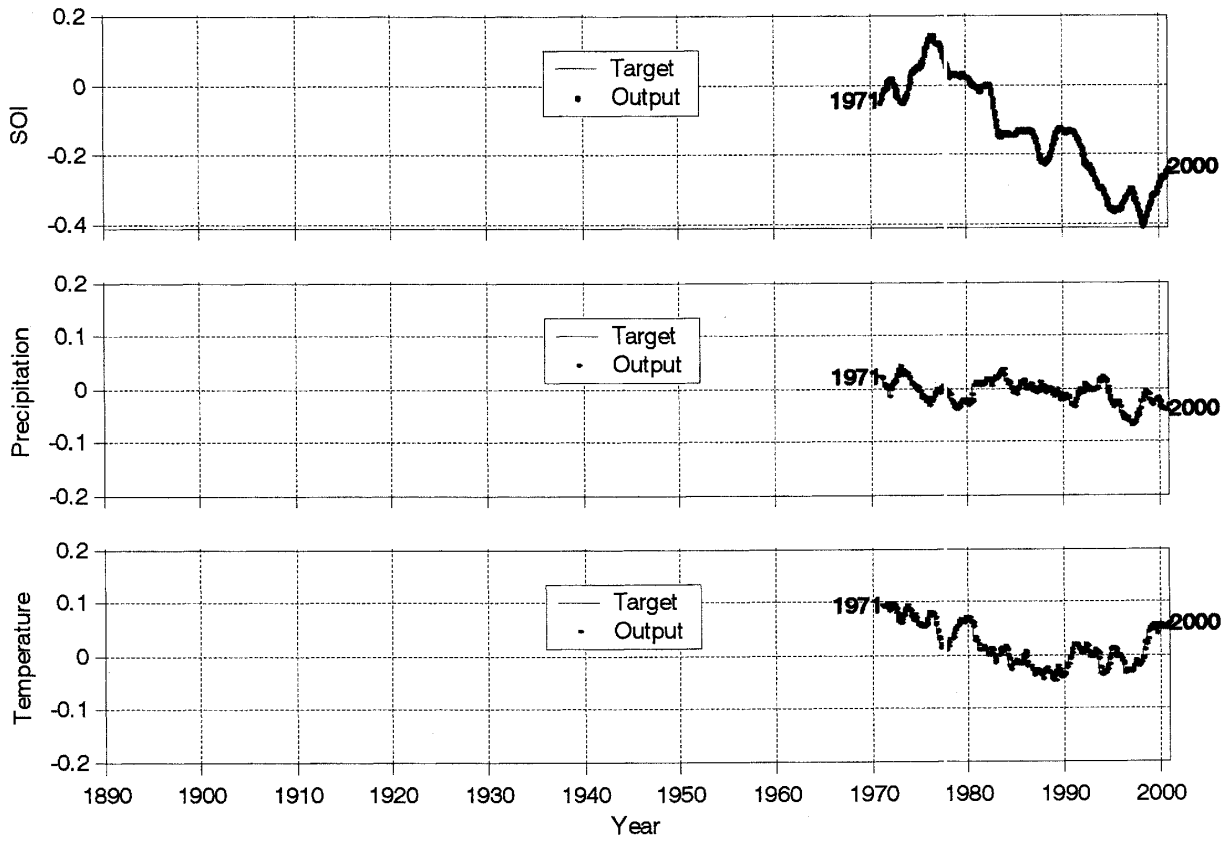

Fig. 16 Observed and predicted values from the artificial neural network with pure linear for transfer function in hidden layer in validation.

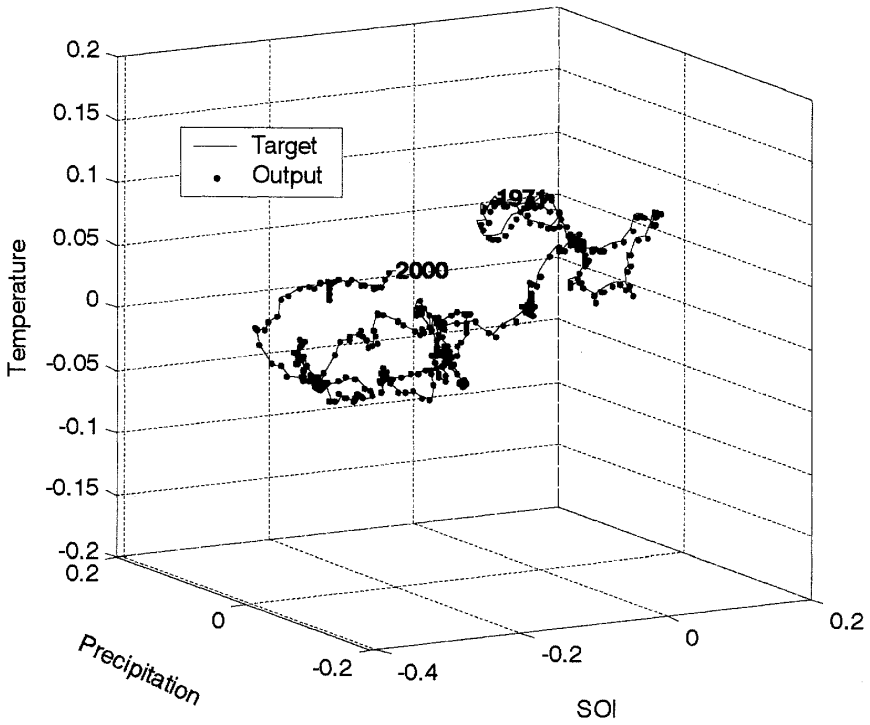

Fig. 17 Three-dimensional phase space representing observed and predicted values in validation of the artificial neural network with pure linear for transfer function in hidden layer.

5. Conclusions and Discussions

ENSO-influence has been considered as it has played a driving force affecting local climate variation, causing great disasters with far distance by teleconnection. It is imperative to understand how the regional driving force has influenced the local variables and how the relationship among them has evolved dynamically.

In the present study, artificial neural networks (ANNs) were employed to show the dynamical behavior of the interaction among them and to predict the interaction. It is apparent that ANNs can obtain its computing power through, first, massively parallel-distributed structure and, second, its ability to learn and therefore generalize. These two information-processing capabilities make it possible for ANNs to solve complex problems and predict more accurately. The remarkable characteristics of ANNs were used to represent the nonlinear relationship among SOI, precipitation and temperature at Fukuoka. The three variables were used for input data simultaneously, after applying the low pass filter to reduce noise contained in the time series. Error back-propagation algorithm was applied to the training phase to identify the weights of the network. There were two types of transfer functions in hidden layer, i.e., hyperbolic tangent and pure linear functions.

The neural network with hyperbolic tangent function in hidden layer showed the limitation in validation that it cannot extrapolate the extreme values beyond the data range for training. Especially, this phenomenon was remarkable on the validation for SOI. However, the network with pure linear function in hidden layer revealed that it could predict well and at the same time, extrapolate the extreme values, which have never occurred in training and testing periods.

Consequently, the performance of identified model of ANNs with pure linear function was considerably successful in testing and validation as well as training. In other words, the

simultaneous predictability of multivariate time series was well performed. The identified neural network model includes the interaction among a regional driving force of ENSO and local hydro-meteorological variables such as precipitation and temperature.

Additionally, the interaction of the three variables was depicted in three-dimensional phase space to see the dynamical variation. Observed and predicted values in training, testing, and validation phases of the identified neural network with pure linear function in hidden layer were used to show the behavior of interaction among variables in time as well as shown as the respective time series plots. Even though generalization of the evolving interaction among them could not formulated, it was considerably meaningful in the sense that the trial to understand the behavior dynamically was performed for the first time considering a regional driving force and local hydro-meteorological variables. Furthermore, it is strongly recommended to carry out the procedure to obtain better understanding of nonlinear dynamics underlain among the variables.

Reference

1) Chiew F. H. S., Piechota T. C., Dracup J. A., and McMahon T. A. 1998, El Niño/Southern Oscillation and Australian rainfall, streamflow and drought: Links and potential for forecasting. J. Hydrol., 204, 138-149.
2) Poveda G., Jaramillo A., Gil M. M., Quiceno, N., and Matilla R. I. 2001, Seasonality in ENSO-related precipitation, river discharge, soil moisture, and vegetation index in Colombia. Water Resour. Res., 37-8, 2169-2178.
3) Gutiérrez F. and Dracup J. A. 2001, An analysis of the feasibility of long-range streamflow forecasting for Colombia using El Niño-Southern Oscillation indicators. J. Hydrol., 246, 181-196.
4) Dracup J. A. and Kahya E. 1994, The relationships between U. S. streamflow and La Niña events. Water Resour. Res., 30-7, 2133-2144.
5) Rodo X., Baert E., and Comin F. A. 1997, Variations in seasonal rainfall in Southern Europe during the present century: relationships with the North Atlantic Oscillation and the El Niño-Southern Oscillation. Clim. Dynamics, 13, 275-284.
6) Yoshino, F. 1999, On the relation between the monthly rainfall in Shikoku island and the El-Niño event, Proc. of Fifth Symposium of Shikoku Branch of JSCE, 90-91.
7) Kawamura A., Eguchi S., and Jinno K. 2000, Cross-correlation between Southern Oscillation Index and precipitation/temperature in Fukuoka, Japan, Proc. of Fresh Perspectives on Hydrology and Water Resources in Southeast Asia and the Pacific, Christchurch, New Zealand, 32-39.
8) Kawamura A., Eguchi S., and Jinno K. 2001, Correlation between Southern Oscillation and monthly precipitation in Fukuoka, Journal of Hydraulic, Coastal and Environmental Engineering, JSCE, 691(II-57), 153-158.
9) Jin Y.-H., Kawamura A., and Jinno K. 2002, Comparison of correlation between categorized SOI and monthly precipitation at Pusan in Korea and at Fukuoka in Japan, Proc. of Korea Water Resources Association, 1251-1256.
10) Kawamura A, McKerchar A. I., Spigel R. H., and Jinno K. 1998, Chaotic characteristics of the Southern Oscillation Index time series. J. Hydrol., 204, 168-181.
11) Haykin S. 1999, Neural networks: A comprehensive foundation. New Jersey: Prentice Hall.
12) Maier H. R. and Dandy G. C. 2000, Neural networks for the prediction and forecasting of water resources variables: a review of modelling issues and applications. Environmen-

tal Modelling & Software, 15, 101-124.
13) Maier H. R. and Dandy G. C. 1997, Determining inputs for neural network models of multivariate time series. Microcom. Civil Eng., 12, 353-368